En-face analysis of the human limbal lymphatic vasculature

Christoph Palme [a], Sajjad Ahmad [b,c,d], Vito Romano [b], Christof Seifarth [a], Bryan Williams [b], Mohit Parekh [d], Stephen B. Kaye [b], Bernhard Steger [a,*]

[a] Department Ophthalmology, Medical University of Innsbruck, Austria
[b] Department of Eye and Vision Science, University of Liverpool, Liverpool, United Kingdom
[c] Moorfields Eye Hospital NHS Foundation Trust, London, UK
[d] Institute of Ophthalmology, University College London, London, UK

ARTICLE INFO

ABSTRACT

Purpose: To describe the location and morphometric characteristics of the human limbal lymphatic vasculature and its relation to the marginal corneal vascular arcades (MCA).
Methods: Ex vivo confocal microscopic (CM) imaging and immunofluorescence double staining for CD-31 and D2-40 of histological en-face sections using 12 preserved human cadaveric corneoscleral discs were performed, followed by a semi-automated morphometric analysis of the two-dimensional vascular network architecture.
Results: Ex vivo CM confirmed the presence of 2 distinct vascular networks. The haematic limbal vascular complex (HLVC) extended further into the cornea, forming typical MCAs. The lymphatic limbal vascular complex (LLVC) was peripheral from the termination of Bowman's layer and was also found to be peripheral to and deeper than the HLVC. LLVC and HLVC were significantly different with respect to vessel diameter, segment length and wall thickness.
Conclusion: The lymphatic vasculature of the human corneoscleral limbal region displays specific morphometric features that allow its differentiation from haematic vessels using CM.

1. Introduction

Confocal microscopy (CM) has been used to describe the anatomy of the human corneoscleral limbus and the limbal stem cell niche both *in vivo* (Falke et al., 2012; Patel et al., 2006; Shortt et al., 2007) and *ex vivo* (Sigal et al. 2016) *with comparable anatomical results.* Yielding high-quality microscopic images of en-face sections in the region of interest, CM offers a unique and non-invasive opportunity to study these structures. While characteristics of the limbal stem cell niche are well described (Falke et al., 2012; Shortt et al., 2007), little attention has been given to the architecture of the limbal microvasculature using CM. Although indocyanine green (ICG) angiography has been used to study the marginal corneal arcades (MCA) (Zheng et al., 2013), CM in contrast to angiography provides important three-dimensional information (Sigal et al., 2016), and details on vessel depth, three-dimensional relation to neighbouring structures and the lymphatic vasculature (Romano et al., 2015).

The anatomical interpretation of *in vivo* CM findings of the healthy human ocular surface is based on the investigator's judgement, as the imaged tissue cannot usually be excised for comparative histological analysis. Currently, subjective interpretation of *in vivo* CM can only be converted into objective parameters by comparative histological sectioning. In the assessment of the human limbus, even the comparison of *in vivo* CM and histology is difficult, because the corneoscleral tissue is rarely excised to allow subsequent histologic sectioning, mandating the use of *ex vivo* tissues for this purpose.

The use of immunofluorescence staining of the limbal region to assess blood vessels and lymphatic vessels, is well established in both animal models and the human eye (Cursiefen et al., 2002; van der Merwe and Kidson, 2010). A recent consensus statement on the detection of lymphatic vessels in the eye concluded, that the presence or absence of erythrocytes or lymph-like fluid is insufficient to discriminate between lymphatic and blood vessels, and that the use of more than one lymphatic endothelial marker or a marker panel is recommended for immunohistochemistry except for regions where the existence of lymphatics is already well established (Schroedl et al., 2014). In compliance

with this recommendation, the aim of this study was to characterize the corneal and limbal lymphatic microvasculature in cadaveric tissue using CM and immunofluorescence.

2. Methods

2.1. Ethical statement

Informed consent for tissue donation and use in research was obtained from the decendent's next of kin and the study adhered to the tenets of the Declaration of Helsinki for experiments involving human tissue. The institutional review board provided approval for this study.

2.2. Tissue specimens

For *ex vivo* CM, 6 corneoscleral tissue specimens stored in cornea cold medium were obtained from normal human donor eyes (mean age 70.2 ± 1.9 years). The corneoscleral buttons were not suitable for transplantation because of a low endothelial cell density (1800 ± 121, minimum 1500, maximum 2000), but originated from donors without any known ocular diseases. The retrieved eyes were enucleated and stored in a cold moist chamber at 2–6° Celsius after a mean post-mortem time of 14.6 ± 4.6 h (min 8, max 18). Corneoscleral buttons were placed in media at 2–6° Celsius for a maximum of 26 h. A 6 mm central corneal punch was used to excise the central cornea and the corneoscleral rim cut into 8 sections. This resulted in a total of 48 limbal and 6 central corneal sections for *ex vivo* CM analysis. The mean storage time in cornea cold medium at the time of *ex vivo* CM was 13 ± 3 days (min 11, max 17).

For immunofluorescence, 6 corneoscleral rim specimens were obtained from tissue used for corneal transplantation, stored in organ culture medium for a mean time of 19 days (min 15, max 24) with a mean post-mortem time of 17 ± 5.4 h (min 14, max 23 h). The mean donor age was 67.6 ± 10.3 years. These rims were radially cut into 8 sections and further processed for immunofluorescence staining as described below.

2.3. Ex vivo confocal microscopy

Laser scanning *ex vivo* CM was performed on all 54 corneal and limbal sections with the Heidelberg Retina Tomograph II Rostock Corneal Module (RCM; Heidelberg Engineering GmBH, Dossenheim, Germany). This microscope utilizes a 670-nm red wavelength diode laser source (Peebo et al., 2011). A 60× objective water immersion lens with a numerical aperture of 0.9 (Olympus, Tokyo, Japan) and a working distance, relative to the applanating cap, of 0.0–3.0 mm was used. The dimensions of each image were 400 × 400 µm and the manufacturers quoted transverse resolution and optical section thickness was 2 µm and 4 µm, respectively. The corneal sections were dried on the endothelial side with a cellulose sponge (Cellulose Spears, Eyetec Ophthalmic Products, Altomed Ltd, UK) and then held fixed in front of the applanation cap. A drop of Viscotears (Carbomer 980, 0.2%; Novartis, North Ryde, NSW, Australia) was used as a coupling agent between the applanating lens cap and the cornea. At a focus depth of 20 µm the sections were first examined from the corneal surface and the focus depth increased until Bowman's layer was identified. The focus was then slowly moved peripherally towards the limbus, until the termination of Bowman's layer was seen. This region was subsequently imaged at a focal depth of between 0 µm and 200 µm. From 5 sections of the central cornea, a full thickness confocal microscopic scan was performed until the level of Descemet's membrane was reached. For all scans the device's "section mode" was performed, which enables instantaneous imaging of a single area of the cornea at a desired depth. Intra-lymphovascular cells were defined as hyperreflective, uniform, intravascular structures with a diameter of 5 µm–11 µm (Peebo et al., 2010).

2.4. Immunofluorescence analysis

For immunofluorescence staining (IMF) samples were fixed in 4% formaldehyde overnight, washed in Tris buffered saline (TBS) and mounted horizontally with Tissue Tek (Dormagen, Germany) OCT compound (Sakura cat 4583) on a specimen disc as follows. A thick layer of OCT compound was frozen on the specimen disc, the position of the specimen disc on the cryostat marked and the OCT compound cut horizontally. The disc was removed and a thin silicon ring placed as a spacer. The sample with some OCT compound was positioned into the ring and frozen rapidly by use of a heat extractor. The mounted samples were cut parallel to the surface at a thickness of 100 µm. The first sections of each sample were transferred in phosphate-buffered saline for immunofluorescence staining to identify blood and lymphatic vessels. All staining steps were done free floating at 4 °C for 24 h. After blocking with 0.3 M Glycin and 5% donkey serum in TBS-T 0,1% buffer, the samples where incubated with Podoplanin (1:300, Dako cat M3619) and CD-31 (1:50, Abcam cat ab28364). The detection of the primary antibodies was undertaken with donkey anti mouse Alexa Fluor 555 (Invitrogen cat A-31570) and donkey anti rabbit Alexa Fluor 488 (Abcam cat ab150111) as secondary antibodies. After washing, the slides were mounted carefully on microscope slides with antifading mounting medium containing 4′,6-diamidino-2-phenylindole (DAPI, Dianova cat SCR-038448). Controls were prepared by omitting one of the two antibodies. Microphotographs where taken on a Zeiss Axio Imager Z2 fluorescence microscope.

2.5. Immunohistochemical analysis

For immunohistochemical staining, the samples were fixed in 4% formaldehyde overnight, washed in PBS and mounted perfectly horizontally with Tissue Tek OCT compound (Sakura cat 4583) on a specimen disc as follows. A thick layer of OCT compound was frozen on the specimen disc, the position of the specimen disc on the cryostat marked and the OCT compound cut horizontally. The disc was removed and a thin silicon ring placed as a spacer. The sample with some OCT compound was positioned into the ring and frozen rapidly by use of a heat extractor. The mounted samples were cut in parallel sections with a thickness of 100 µm. The first slides of each sample were transferred into PBS and used for LYVE1 (Zytomed cat RBK014-05) and CD-31 (Dako cat M3823) staining to identify lymphatic and blood vessels. An Ultravision LP Kit (thermos scientific Cat. TL-0L60-HL) was used to stain the free floating sections at 4 °C. LYVE1 (1:50) was used and visualized with DAB (Roche, cat. 11,718,096,001). The sections were then heated in citrate buffer for 5 min at 97 °C, cooled before staining with anti CD31 antibody (1:200) and visualized with AEC (Thermo scientific, cat. TA-060-SA). The counterstain of the nuclei was done with diluted Harris haematoxylin (Roth, cat. X903.1). For control specimens one or both antibodies were omitted.

2.6. Semi-automated vessel analysis

In order to describe and compare morphometric characteristics of haematic and lymphatic limbal vascular networks, both 2-dimensional *ex vivo* CM image reconstructions and immunofluorescence micrographs were morphometrically analyzed and compared. For this purpose, two-dimensional CM image reconstructions and IMF sections were exported in BMP format for the purpose of quantitative analysis using an in-house automated program written in Matlab R14 (The Mathworks Inc., Natick, MA), as previously described (Zheng et al., 2013). The quantitative information allows derivation of vessel diameter, number of bifurcations, bifurcation angles, measures of tortuosity, ratio between length and diameter.

Semi-automated vessel analysis consists of the following process steps. The first step involved the identification of limbus manually on the image to measure the corneal diameter in pixels. This was followed
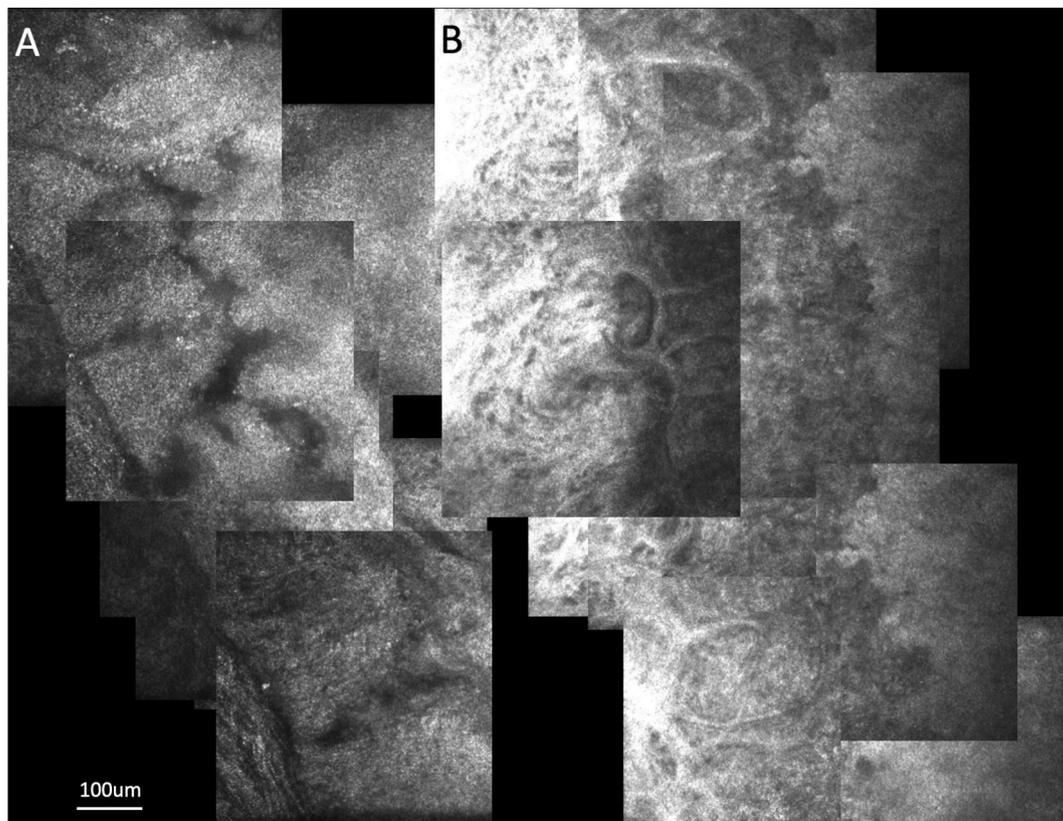
Fig. 1. Confocal microscopic two-dimensional reconstruction showing the lymphatic limbal vascular complex (LLVC, Fig. 1A, focus depth 34–40 μm), and the haematic limbal vascular complex (HLVC, 1 B, focus depth 20–26 μm). After imaging the HLVC, the focal plane was lowered by approximately 20 μm to visualize the HLVC. The termination of Bowman's layer is seen in proximity to the MCA's terminal loops in Fig. 1B (white arrow). The LLVC is characterized by large lumens with indistinguishable vessel walls, and no obvious formation of arcades. The HLVC is hyperreflective, shows a comparably thinner vessel diameter with very small vascular lumen, no visible intravascular cells and forms well-defined round vascular arcades as previously described (Zheng et al., 2013).

by estimation of pixel resolution (mm/pixel), defined as the ratio between the diameter of the cornea and the number of pixels. A sub-image containing all the corneal vessels was defined by hand and enhanced through a Gaussian filter to remove noise, followed by the application of selective enhancement filters initially described by Li et al. (Li et al., 2003), to the smoothed image to enhance all the potential vessels as linear structures. This filter was adopted for its simplicity and effectiveness. The enhanced image was then converted to a binary image in which all the pixels with values higher than a predefined value were marked as 1 (vessel pixels), the rest as 0 (background pixels). The binary image was further cleansed by removing objects smaller than 10 pixels. Linear measurements were made according to the number of pixels and the resolution of pixels in x and y axes. After segmentation of the corneal vessels, a three-step automatic analysis process was adopted to quantify the geometric property of the vasculature tree structure by adapting a well-established semiautomatic method described by Martinez-Perez et al., (2002). First, the centerlines of the segmented vessels were determined by a mathematical morphologic thinning operation. The significance points (branch points and terminal points) were identified and used to segment the vascular tree into individual segments. For each vessel segment, its geometric features (length, area, diameter along the path, average diameter, and tortuosity) were measured and used to describe the overall vessel properties.

2.7. Statistical analysis

Quantitative measurements were reported as mean ± SD, minimum and maximum. Two-sided t-tests were used and a P value of less than 0.05 were considered statistically significant. Bland-Altman plots were used to assess agreement between vessel parameter measurements of CM and histological images and the mean of the observed differences, with 95% limits of agreement (LOA) and 95% confidence interval for LOA were reported.

3. Results

3.1. Ex vivo confocal microscopy

The central corneal thickness as measured by *ex vivo* CM was 609 ± 31 μm. The central corneal epithelium had a thickness of 23 ± 12 μm. Epithelial cell morphology was remarkable for hyperreflectivity throughout all cell layers and barely visible cell nuclei in the basal cell layer. In no case could a typical surface cell layer with large epithelial cells carrying visible cell nuclei be identified. Bowman's layer was clearly visible in all specimens but the sub-basal nerves were seen in only 2 specimens of central corneal tissue. No dendritic cells in the central corneal basal epithelial cell nor the Bowman's layer were observed. The corneal stroma revealed unremarkable keratocytes with intermittent visible stromal nerves. Intercellular space was wide, consistent with mild stromal edema. The presence of anterior stromal microdots (Steger et al., 2014) was noted in 4 of 6 central corneal specimens. Imaging of the endothelium was not possible at sufficient quality for quantitative analysis, as the endothelium was touched with a cellulose sponge for *ex vivo* CM.

The vessel wall of the haematic limbal vascular complex (HLVC) appeared hyperreflective with an almost indistinguishable vascular lumen; no vessel walls were identified in the lymphatic limbal vascular complex (LLVC). No intravascular cells were seen in the HLVC in any case, while round, nucleated intravascular cells were identified in 12 of 21 corneal samples with visible LLVC. Mean vascular diameters were
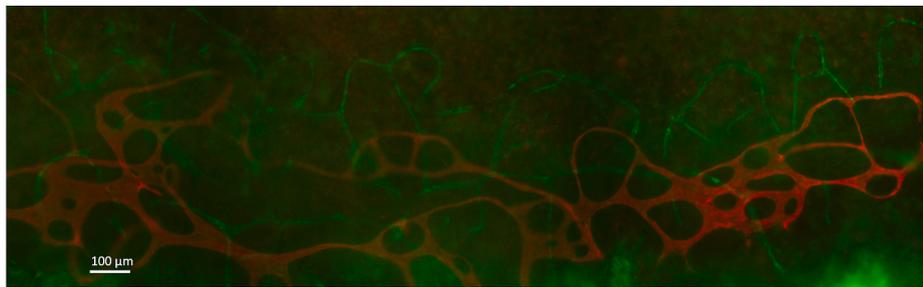
Fig. 2. Immunofluorescence micrograph showing a D2-40 and CD-31 positive limbal lymphatic vascular complex (red) and a CD31 positive haematic limbal vascular complex (HLVC, green). The HLVC extends further into the cornea compared to the lymphatic vessels. (For interpretation of the references to color in this figure legend, the reader is referred to the Web version of this article.)

significantly different between HLVC and LLVC, 16 ± 8 μm versus 29 ± 32 μm (p = 0.031), respectively. A confocal microscopic two-dimensional reconstruction of the HLVC and LLVC is shown in Fig. 1.

3.2. Immunofluorescence analysis

Ex vivo CM of 48 limbal sections showed the mean corneal limbal epithelial thickness of 31 ± 17 μm with limbal epithelial crypts (Shortt et al., 2007) between the palisades of Vogt reaching a maximum depth of 79 μm. The termination of Bowman's layer was identified in 39 of 48 sections. The HLVC was identified in 38 of 40 sections at a mean depth of 24 ± 9 μm. Its centripetal extension usually correlated with the termination of Bowman's layer, located at the level of basal epithelial cells or Bowman's layer. A second morphologically distinct vascular network was identified in 21 of 40 sections. It was characterized by a more peripheral and deeper location of its terminal vascular loops compared to HLVC with a mean depth of 43 ± 12 μm (p = 0.004), corresponding to a presumed LLVC. The depth difference is illustrated in Supplementary Fig. S1. Mean vascular diameters were significantly different between these two vascular complexes: 13 ± 8 μm for HLVC versus 36 ± 38 μm for LLVC (p = 0.012). An immunofluorescene micrograph depicting the LLVC in relation to the HLVC is shown in Fig. 2.

3.3. Semi-automated vessel morphometry

The calculated tortuosity index was not significantly different between the LLVC and HLVC on neither *ex vivo* CM (1.04 ± 0.4 versus 1.05 ± 0.3; p = 0.85) nor IMF (1.04 ± 0.8 versus 1.01 ± 0.8; p = 0.81). Similarly, the calculated mean intersegmental angle was not significantly different between LLVC and HLVC on neither *ex vivo* CM (101.4 ± 34 versus $116.3 \pm 48°$; p = 0.09) nor IMF (102.4 ± 43 versus $112.3 \pm 31°$; p = 0.16). Significant differences between the LLVC and the HLVC were found for vessel segment length using both *ex vivo* CM (54.3 ± 16 vs. 65.4 ± 25 pxl; p = 0.04) and IMF (52.1 ± 13 vs. 64.0 ± 21 pxl; p = 0.01), both confirming longer vessel segments in vascular compared to lymphatic vascular networks.

4. Discussion

As far as we are aware, this is the first study to characterize the human corneal limbal blood and lymphatic microvasculature by comparison of *ex vivo* CM and en-face IMF analysis. Our findings have established morphometric characteristics that may aid in the differentiation of lymphatic and haematic vascular corneal networks using *in vivo* CM. This is clinically relevant, because corneal graft rejection remains one of the leading causes of graft failure, despite ongoing advances in corneal transplantation surgery and graft management.[15] Corneal vascularization is the single most important risk factor for corneal graft rejection.[16] It is the lymphatic vessels, however, not the haematic vessels that are the principal mediators of corneal graft rejection (Dietrich et al., 2010). Several attempts have been made to

visualize corneal lymphatics *in vivo*. We reported an angiography-based method using digital subtraction analysis to image corneal lymphatic vessels *in vivo* (Romano et al., 2015). While this method allows the depiction of corneal lymphatics *in vivo*, it is limited by poor reproducibility due to angle and focus deficiencies of corneal angiograms. Likewise, a recent publication using intrastromal fluorescein injection is too invasive to be used in clinical practice (Le et al., 2018). Peebo et al. were among the first to compare histologic and *in vivo* CM images of identical corneal regions in rats. They showed that lymphatic vessels display no discernible vessel wall, have a dark lumen containing reflective cells (presumed leukocytes) of roughly uniform size that were larger than most particles observed in blood vessel and differed in their fluid-odynamics (Peebo et al., 2010). Horstmann et al. demonstrated the feasibility of high resolution optical coherence tomography to image lymphatic vessels *in vivo*, using a murine model for corneal neovascularization (Horstmann et al., 2017). They established similar morphologic characteristics for lymphatic vessels, such as the appearance of the vessels as tubular structures, darker than the surrounding tissue and empty or sparsely filled with cells, showing only very slow if any flow compared to blood vessels.

In the present study we can confirm from en-face analysis, that HLVC and LLVC are morphometrically different in their segment length and vessel diameters. Along with established *in vivo* confocal characteristics of corneal lymphatic vessels including indistinguishable vessel walls, presence of large intravascular cells and absence of visible cell flow (Peebo et al., 2011; Peebo et al., 2010), these new parameters may increase the specificity of *in vivo* lymphatic vascular imaging.

The clinical applicability of results of our study are limited in that CM was used to assess limbal corneal tissue *ex vivo*, while conclusions are made on the use of this technique *in vivo*. Vascular lumen may be different *in vivo* compared to the experimental setting and it is unclear to what extent postmortem changes affect the architecture and morphometry of the limbal lymphatic vasculature. Likewise, intravascular cell content and traffic cannot be not be sufficiently described *ex vivo*. In addition, the lack of a direct correlation of *ex vivo* CM and IMF images in the same tissue may further limit the validity of our results. The use of unaltered limbal-corneal tissue, however, for both analytical methods did allow sufficient comparison.

A strength of this research is its compliance with a recent consensus statement defining IMF as a prerequisite for the identification of ocular lymphatic vessels for scientific purposes (Schroedl et al., 2014). In the current study, correlating *ex vivo* CM and IMF, we were therefore able to confirm and analyze lymphatic vessels in compliance with current standards of lymphatic vascular research.

Our findings are not directly applicable to pathological corneal neovessels, as the morphological architecture and extent of both lymphatic and haematic corneal neovessels is highly dynamic during angiogenesis and angio-regression (Faraj et al., 2015; Romano et al., 2015).

In conclusion, this study describes the precise 3-dimensional anatomical location of the human LLVC in relation to the HLVC.

Adding to the already known morphological differences between haematic and lymphatic vasculature e.g. vessel wall thickness and intracellular content, we describe novel morphological differences between LLVC and HLVC in vessel segment length and vessel diameters, supported by IMF correlation. As specific anti-lymphangiogenetic treatments continue to evolve, feasible clinical imaging methods are needed to monitor angioregressive treatments and the assessment of the individuals risk, for example, corneal graft rejection (Bock and Cursiefen, 2017; Bock et al., 2013; Maehana et al., 2016). Our results show, that CM enables the identification and analysis of lymphatic vessels in the human corneoscleral limbal region. Pending further study on the applicability of these results to corneal neovascularization, IVCM aided by angiography may be suitable for clinical application.

Declaration of competing interest

The results of this research were presented at the 2019 ARVO annual meeting in Vancouver, CA.

The authors declare that there is no conflict of interests regarding the publication of this article. No funding was obtained for the conduction of this research.

Appendix A. Supplementary data

Supplementary data to this article can be found online at https://doi.org/10.1016/j.exer.2020.108278.

References

Bock, F., Cursiefen, C., 2017. [Anti(lymph)angiogenic strategies to improve corneal graft survival]. Klin. Monatsbl. Augenheilkd. 234, 674–678.

Bock, F., Maruyama, K., Regenfuss, B., Hos, D., Steven, P., Heindl, L.M., Cursiefen, C., 2013. Novel anti(lymph)angiogenic treatment strategies for corneal and ocular surface diseases. Prog. Retin. Eye Res. 34, 89–124.

Cursiefen, C., Schlötzer-Schrehardt, U., Küchle, M., Sorokin, L., Breiteneder-Geleff, S., Alitalo, K., Jackson, D., 2002. Lymphatic vessels in vascularized human corneas: immunohistochemical investigation using LYVE-1 and podoplanin. Invest. Ophthalmol. Vis. Sci. 43, 2127–2135.

Dietrich, T., Bock, F., Yuen, D., et al., 2010. Cutting edge: lymphatic vessels, not blood vessels, primarily mediate immune rejections after transplantation. J Immunol Baltim Md 1950 184, 535–539.

Falke, K., Prakasam, R.K., Guthoff, R.F., Stachs, O., 2012. [In vivo imaging of limbal epithelium and palisades of Vogt]. Klin. Monatsblätter Augenheilkd. 229, 1185–1190.

Faraj, L.A., Said, D.G., Al-Aqaba, M., Otri, A.M., Dua, H.S., 2015. Clinical evaluation and characterisation of corneal vascularisation. Br. J. Ophthalmol.

Horstmann, J., Schulz-Hildebrandt, H., Bock, F., Siebelmann, S., Lankenau, E., Hüttmann, G., Steven, P., Cursiefen, C., 2017. Label-free in vivo imaging of corneal lymphatic vessels using microscopic optical coherence tomography. Invest. Ophthalmol. Vis. Sci. 58, 5880–5886.

Le, V.N.H., Hou, Y., Horstmann, J., Bock, F., Cursiefen, C., 2018. Novel method to detect corneal lymphatic vessels in vivo by intrastromal injection of fluorescein. Cornea 37, 267–271.

Li, Q., Sone, S., Doi, K., 2003. Selective enhancement filters for nodules, vessels, and airway walls in two- and three-dimensional CT scans. Med. Phys. 30, 2040–2051.

Maehana, S., Nakamura, M., Ogawa, F., Imai, R., Murakami, R., Kojima, F., Majima, M., Kitasato, H., 2016. Suppression of lymphangiogenesis by soluble vascular endothelial growth factor receptor-2 in a mouse lung cancer model. Biomed Pharmacother Biomedecine Pharmacother 84, 660–665.

Martinez-Perez, M.E., Hughes, A.D., Stanton, A.V., Thom, S.A., Chapman, N., Bharath, A.A., Parker, K.H., 2002. Retinal vascular tree morphology: a semi-automatic quantification. IEEE Trans. Biomed. Eng. 49, 912–917.

Patel, D.V., Sherwin, T., McGhee, C.N.J., 2006. Laser scanning in vivo confocal microscopy of the normal human corneoscleral limbus. Invest. Ophthalmol. Vis. Sci. 47, 2823–2827.

Peebo, B.B., Fagerholm, P., Lagali, N., 2011. In vivo confocal microscopy visualization of presumed lymph vessels in a case of corneal transplant rejection. Clin. Exp. Ophthalmol. 39, 832–834.

Peebo, B.B., Fagerholm, P., Traneus-Röckert, C., Lagali, N., 2010. Cellular-level characterization of lymph vessels in live, unlabeled corneas by in vivo confocal microscopy. Invest. Ophthalmol. Vis. Sci. 51, 830–835.

Romano, V., Steger, B., Zheng, Y., Ahmad, S., Willoughby, C.E., Kaye, S.B., 2015. Angiographic and in vivo confocal microscopic characterization of human corneal blood and presumed lymphatic neovascularization: a pilot study. Cornea 34, 1459–1465.

Schroedl, F., Kaser-Eichberger, A., Schlereth, S.L., et al., 2014. Consensus statement on the immunohistochemical detection of ocular lymphatic vessels. Invest. Ophthalmol. Vis. Sci. 55, 6440–6442.

Shortt, A.J., Secker, G.A., Munro, P.M., Khaw, P.T., Tuft, S.J., Daniels, J.T., 2007. Characterization of the limbal epithelial stem cell niche: novel imaging techniques permit in vivo observation and targeted biopsy of limbal epithelial stem cells. Stem Cells Dayt Ohio 25, 1402–1409.

Sigal, I.A., Steele, J., Drexler, S., Lathrop, K.L., 2016. Identifying the palisades of Vogt in human ex vivo tissue. Ocul. Surf. 14, 435–439.

Steger, B., Speicher, L., Philipp, W., Bechrakis, N.E., 2014. In vivo confocal microscopic characterisation of the cornea in chronic graft-versus-host disease related severe dry eye disease. Br. J. Ophthalmol.

van der Merwe, E.L., Kidson, S.H., 2010. Advances in imaging the blood and aqueous vessels of the ocular limbus. Exp. Eye Res. 91, 118–126.

Zheng, Y., Kaye, A.E., Boker, A., et al., 2013. Marginal corneal vascular arcades. Invest. Ophthalmol. Vis. Sci. 54, 7470–7477.